LETTER

Nanoscale magnetic ratchets based on shape anisotropy

To cite this article: Jizhai Cui *et al* 2017 *Nanotechnology* **28** 08LT01

IOP Publishing
Letters
Nanotechnology
Nanotechnology 28 (2017) 08LT01 (10pp)
doi:10.1088/1361-6528/aa56d4

Letter

Nanoscale magnetic ratchets based on shape anisotropy

Jizhai Cui[1], Scott M Keller, Cheng-Yen Liang, Gregory P Carman and Christopher S Lynch[2]

Department of Mechanical and Aerospace Engineering, University of California, Los Angeles, CA 90095, United States

E-mail: cslynch@seas.ucla.edu

Received 12 November 2016, revised 18 December 2016
Accepted for publication 5 January 2017
Published 19 January 2017

Abstract

Controlling magnetization using piezoelectric strain through the magnetoelectric effect offers several orders of magnitude reduction in energy consumption for spintronic applications. However strain is a uniaxial effect and, unlike directional magnetic field or spin-polarized current, cannot induce a full 180° reorientation of the magnetization vector when acting alone. We have engineered novel 'peanut' and 'cat-eye' shaped nanomagnets on piezoelectric substrates that undergo repeated deterministic 180° magnetization rotations in response to individual electric-field-induced strain pulses by breaking the uniaxial symmetry using shape anisotropy. This behavior can be likened to a magnetic ratchet, advancing magnetization clockwise with each piezostrain trigger. The results were validated using micromagnetics implemented in a multiphysics finite elements code to simulate the engineered spatial and temporal magnetic behavior. The engineering principles start from a target device function and proceed to the identification of shapes that produce the desired function. This approach opens a broad design space for next generation magnetoelectric spintronic devices.

S Online supplementary data available from stacks.iop.org/NANO/28/08LT01/mmedia

Keywords: magnetic shape anisotropy, nanomagnetics, magnetoelectrics, multiferroics

(Some figures may appear in colour only in the online journal)

1. Introduction

In this article, we present shape anisotropy based designs of nanomagnets that can achieve 180° deterministic magnetization rotation driven by piezoelectric strain through the strain-mediated magnetoelectric (ME) effect, like magnetic ratchets. The design process led to two novel shapes, 'peanut' and 'cat-eye', which are discussed in detail. The ME effect is attracting considerable research interest due to its low energy consumption and high coupling coefficient relative to other magnetization control methods such as applying magnetic field and spin-polarized current injection [1, 2]. ME driven nanomagnets (nanoscale magnetic elements) can store bit information without any standby power dissipation, offering unprecedented power efficiency, and thus have high potential for implementation in the next generation of spintronic devices [3, 4]. Magnetic anisotropy, an effect with multiple contributions including strain, shape and crystalline structure; determines the degree to which the magnetization direction produces a minimum free energy [5]. The geometric shape of nanomagnets influences the magnetization distribution through magnetic shape anisotropy. This effect can be used to create a controllable magnetic domain pattern that dominates the dynamic magnetic response [6]. Previous research has

[1] Present address: Laboratory for Mesoscopic Systems, Department of Materials, ETH Zurich, 8093 Zurich, Switzerland.
[2] Author to whom any correspondence should be addressed.

experimentally and computationally explored the magnetic shape anisotropy of nanomagnets in highly symmetric shapes, like circles, ellipses, polygons [7], rings [8–10], and even some uncommon shapes like Reuleaux triangles [11]; with emphasis on their integration into device designs. For example, magnetic non-volatile memory and magnetic logic elements have used single domain nanomagnets with bi-stable magnetization states in elliptical [12–14] and quadrilateral [2, 15] shapes with two-fold symmetry. Ferromagnetic rings with geometric center-symmetry have been used in studies of fundamental magnetization behavior such as domain wall trapping [16] and domain wall velocity [17], and have also been proposed for applications like computer memory [18] and nanoscale particle delivery systems [19, 20]. Optimizing the shape of nanomagnets provides an opportunity to significantly improve their functionality. Since magnetic shape anisotropy relates the geometric shape of the nanomagnets to their magnetic behavior, the shape can be tailored to obtain the magnetic anisotropy required for specific applications.

Manipulating magnetization through the strain-mediated ME effect presents challenges when the goal is to achieve 180° magnetization rotation. Magnetic field, a *directional* vector effect, can induce a 180° magnetization switching of a single domain nanomagnet, when applied opposite to the original magnetization direction. However, strain cannot easily induce such 180° full magnetization switching. Considering solely the strain-induced magnetic anisotropy, the strain, a uniaxial effect, can induce at most a 90° reorientation of the magnetization vector [21]. Achieving a full 180° magnetization rotation using strain has been considered a 'fundamental challenge' [22]. Previous researchers achieved strain-mediated electrically driven 180° magnetization switching in single domain nanomagnets on a piezoelectric substrate using magnetocrystalline anisotropy (MCA) [23], dynamic magnetization precession [24–26], a four-electrode design on a piezoelectric requiring application of two different stain fields [27, 28], a flower-shaped nanomagnet also requiring application of two different strain fields [22] and a square-shaped nanomagnet with a bias-field-induced uniaxial magnetic anisotropy [29]. A multi-electrode design creating localized strain in a piezoelectric is a possible method to force a 180° magnetization reorientation of a magnetic ring in the 'onion' state with two head-to-head domain walls [30–32]. All of these approaches involve breaking uniaxial symmetry using either special material properties, e.g. MCA from epitaxial magnetic materials; or complicated device design, e.g. applying piezostrain several times in different orientations to complete a full 180° rotation; and thus complicate the fabrication process.

Simulation tools that capture the spatial and temporal magnetic response of complex shapes to strain are required to engineer shapes with desired magnetic behavior. In most previous work the contribution of demagnetization field is included by assuming a uniform demagnetization coefficient, and a uniform demagnetization field H_d is assumed equal to this coefficient times the magnetization. In general, the demagnetization coefficient is a rank two tensor and is not spatially homogeneous. The approach presented in this paper demonstrates the use of 'simple' structures with uniform demagnetization coefficients to estimate the geometry of much more complex forms with non-uniform demagnetization effects. Finite element methods are then used to simulate the fully dynamic spatial and temporal evolution of the magnetization to confirm and fine tune device functionality.

The perturbation of well understood shapes followed by simulations led to the design of the novel 'peanut' and 'cat-eye' architected geometric shapes that offer the ability to produce 180° magnetization reorientation by applying *a single piezostrain pulse*. Applying the same strain field again induces a second 180° magnetization rotation, resulting in a complete 360° rotation. The design takes advantage of magnetic shape anisotropy and can be implemented using any magnetostrictive thin films. The 'peanut' and 'cat-eye' were designed as a simple two-terminal device with a voltage-controlled piezoelectric substrate. In both designs the magnetization only rotates clockwise (CW) and thus forms a magnetic ratchet. We present these two designs separately. In each case we begin with the shape architecting process. This is followed by strain coupled micromagnetics simulations that were used to characterize the magnetic behavior in response to piezoelectric strain. Using this methodology gives designers a technique to rapidly achieve a design target and minimizes the amount of modeling required to verify the design.

In the dynamic simulations, the magnetic domain structure is described by the spatially distributed magnetization $M = M_s\,(m_x, m_y, m_z)$, where M_s and m_x, m_y, m_z represent the saturation magnetization and the direction cosines, respectively. The equation of motion describing the evolution of the magnetization temporally is the Landau–Lifshitz–Gilbert (LLG) equation [5],

$$\frac{\partial \underline{m}}{\partial t} = -\mu_0\gamma(\underline{m} \times \underline{H}_{\text{eff}}) + \alpha\left(\underline{m} \times \frac{\partial \underline{m}}{\partial t}\right), \tag{1}$$

where γ and α are the gyromagnetic ratio and the damping coefficient, respectively. $\underline{H}_{\text{eff}} = \underline{H}_{\text{ex}} + \underline{H}_{\text{el}} + \underline{H}_d$, is the effective magnetic field. The simulations assume a polycrystalline nickel material and no external magnetic field, so there are no contributions to the effective magnetic field for these effects. The exchange field term is given by

$$\underline{H}_{\text{ex}} = \frac{2A_{\text{ex}}}{\mu_0 M_s}\Delta\underline{m}. \tag{2}$$

The demagnetization field $\underline{H}_d$ is determined from Ampere's law $\nabla \times \underline{H}_d = 0$ and Gauss's law $\nabla \cdot \underline{B} = 0$ with the constitutive relation $\underline{B} = \mu_0(\underline{H}_s + M_s\underline{m})$. This implies a magnetic potential ϕ such that, $\underline{H}_d = -\nabla\phi$ and $\nabla^2\phi = \nabla \cdot (M_s\underline{m})$ which governs $\underline{H}_d$. The total strain $\underline{\underline{\varepsilon}}$ in a ferromagnetic material is composed of a magnetic eigenstrain, $\underline{\underline{\varepsilon}}^m(\underline{m})$ and elastic strain, $\underline{\underline{\varepsilon}}^{\text{el}}$, contributions with total strain $\underline{\underline{\varepsilon}} = \underline{\underline{\varepsilon}}^m(\underline{m}) + \underline{\underline{\varepsilon}}^{\text{el}}$ where $\underline{\underline{\varepsilon}}^m = \underline{\underline{\underline{\lambda}}}^m\underline{m}\underline{m}^T$ is the strain associated with local magnetization changes in the absence of stress, and $\underline{\underline{\underline{\lambda}}}^m$ is the magneto-mechanical coupling tensor [33–35]. The total strain $\underline{\underline{\varepsilon}}$ is related to the displacement $\underline{u}$ by $\underline{\underline{\varepsilon}} = \frac{1}{2}(\nabla\underline{u} + (\nabla\underline{u})^T)$ and the stress tensor $\underline{\underline{\sigma}}$ is related to the

elastic strains by $\underline{\underline{\sigma}} = \underline{\underline{\underline{\underline{C}}}}\underline{\underline{\varepsilon}}^{el} = \underline{\underline{\underline{\underline{C}}}}[\underline{\underline{\varepsilon}} - \underline{\underline{\varepsilon}}^{m}(\underline{m})]$ where the stress distribution is governed by the elastodynamic equation

$$\rho\frac{\partial^2 \underline{u}}{\partial t^2} - \nabla \cdot \underline{\underline{\sigma}} = 0 \tag{3}$$

with mass density ρ. This leads to

$$\underline{H}_{me} = -\frac{1}{\mu_0 M_s}\underline{\underline{\underline{\underline{C}}}}(\underline{\underline{\varepsilon}} - \underline{\underline{\varepsilon}}^{m}(\underline{m})) \cdot \frac{\partial \underline{\underline{\varepsilon}}^{m}(\underline{m})}{\partial \underline{m}}. \tag{4}$$

These governing equations and boundary conditions are implemented within a finite element framework to simulate the spatial and temporal evolution of magnetization. For a more detailed description of the finite element model see [36].

2. The 'peanut' shaped nanomagnet

The 'peanut' shaped nanomagnet was developed as a single domain magnetic element that can achieve deterministic 180° magnetization reorientation controlled by electric-field-induced strain on a piezoelectric substrate. For a typical uniaxial nanomagnet, like an ellipse, strain-mediated magnetization control is not deterministic. Polycrystalline Ni (with zero volume average MCA) is the magnetic material used in the design unless noted otherwise. A thin-film magnetic element with all three-dimensions on a nanometer length scale (about <300 nm in lateral size and <50 nm in thickness for Ni) forms an in-plane single domain in ground state [14, 37]. A single domain circular nanomagnets does not have in-plane shape anisotropy because all in-plane magnetization directions are geometrically identical [38]. For an elliptical shaped nanomagnet, the magnetic easy axis (EA) and hard axis (HA) are perpendicular to each other, aligning with the geometric major axis and minor axis, respectively [5]. This is due to the magnetic shape anisotropy: the demagnetization field is much larger along the minor axis than along the major axis. Applying a piezoelectric biaxial strain field to the ellipse, compressive strain along one direction and tensile strain in the perpendicular in-plane direction, we can induce a new EA through the magnetoelastic effect [5]. For a material like Ni with negative magnetostriction, the strain-induced EA aligns with the compressive strain direction. If sufficient compressive strain is applied along the original HA direction (geometric minor axis), the magnetization is forced to rotate by 90° from its original EA to this new strain-induced EA (geometric minor axis). When the piezoelectric strain is released, the magnetization rotates back to its original EA (geometric major axis). There is an equal probability of the magnetization rotating toward the original direction or in the opposite direction due to the symmetry. This leads to a total of 0° or 180° magnetization switching, respectively [14]. Hence, for geometric shapes like an ellipse, with the EA and HA perpendicular to each other, the strain-mediated electrically driven magnetization switching process is not deterministic.

Magnetic anisotropy can be induced resulting in a non-perpendicular EA and HA relative orientation. This enables 180° deterministic magnetization rotation in response to piezoelectric biaxial strain [29]. The mechanism is described with reference to figure 1. Before applying piezostrain, the magnetization aligns with the EA shown as the solid red arrow along the blue EA as shown in figure 1(a). As biaxial strain is applied, the tensile strain in the vertical direction makes the vertical axis harder, and the compressive strain in the horizontal direction makes the horizontal axis easier. This effect increases as the strain amplitude is increased, pushing the magnetization clockwise. When sufficient piezoelectric biaxial strain is applied (green arrows), the strain-induced changes to the EA and HA push the magnetization past the original shape controlled HA, rotating it into alignment with the compressive strain direction. Hence the magnetization will rotate CW away from the tensile strain direction towards the compressive strain direction, as the dashed red arrow in figure 1(a) shows. At lower strain amplitudes, there is a metastable state between the strain induced HA in the vertical direction and the shape induced HA. The magnetization does not rotate until sufficient strain is applied to eliminate this metastable state.

After the piezostrain is released, the magnetization reorientation is governed by the original EA and HA, causing the magnetization to rotate away from the original HA and align with the EA, as shown in figure 1(b). Hence with this type of magnetic anisotropy, applying and releasing piezoelectric biaxial strain can induce a 180° deterministic CW magnetization rotation. Similarly, starting from figure 1(b), applying the same strain field will result in the magnetization again rotating CW with the magnetization aligned with the compressive strain direction, as shown in figure 1(c). Releasing the applied piezostrain, the magnetization rotates CW again towards its original EA, moving back to its original direction. This is a second 180° CW magnetization rotation, and in total a 360° CW magnetization rotation can be achieved by applying the same piezoelectric strain field twice. Note that the magnetization can never rotate counterclockwise (CCW) in response to piezostrain with this geometry. A nanomagnet with such magnetic anisotropy has the ability of achieving strain-mediated electrically driven deterministic 180° magnetization rotation.

The 'peanut' shaped nanomagnet was engineered with the magnetic anisotropy described above. The mechanism bridging geometric shape of an ellipse and its magnetic anisotropy is: magnetic EA and HA follow geometric major and minor axes, respectively. In figure 2(a), the ellipse is divided into four quadrants separated by major and minor axes, colored according to quadrant. Starting with an ellipse, we then rotated the major and minor axes to change the angle between the magnetic EA and HA. This produced the shape shown in figure 2(b). The four parts of the outer boundary separating major and minor axes corresponds to the four quadrants with same color in figure 2(a). This new shape is referred to as 'peanut' due to geometric similarity. Figure 2(c) demonstrates the layout of a strain-mediated ME device incorporating the 'peanut' shaped nanomagnet. Single crystal $\langle 011 \rangle$ cut $[Pb(Mg_{1/3}Nb_{2/3})O_3]_{0.66}$-$[PbTiO_3]_{0.34}$ (PMN-PT) is used as piezoelectric substrate. Applying voltage across the substrate thickness induces compressive strain and tensile

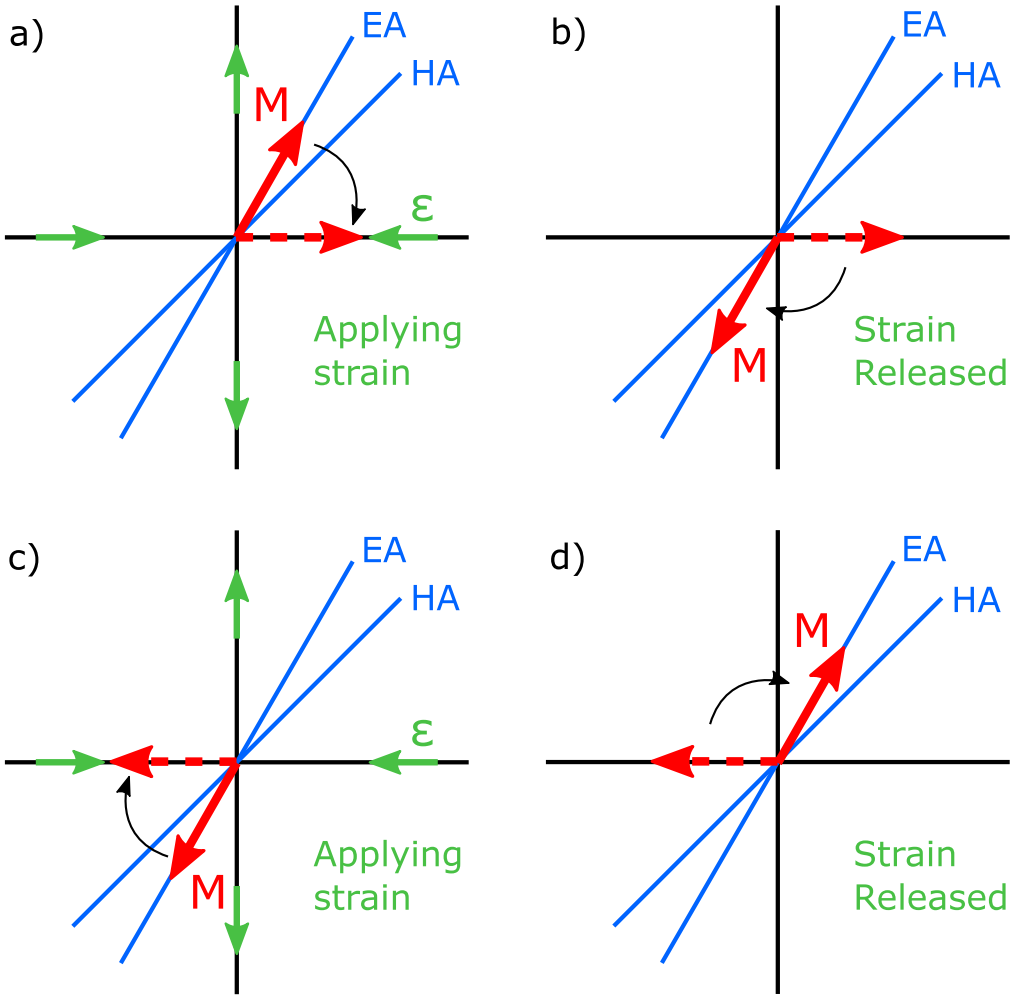

Figure 1. The target magnetic anisotropy with the ability of achieving 180° strain-mediated magnetization rotation under a single piezostrain actuation. (a) and (c) Magnetization (red arrow) rotates away from the EA towards compressive strain direction in response to piezoelectric biaxial strain, crossing over the HA. (b) and (d) Magnetization rotates to the new direction along EA when the strain is released. From (a) to (b) and from (c) to (d), magnetization is rotated 180° CW by applying piezostrain once. From (a) to (d), magnetization is rotated 360° CW in total by applying the same strain field twice.

strain along the [100] and [01$\bar{1}$] directions respectively, providing biaxial strain [39]. Experiments have shown that piezoelectric biaxial strain $\varepsilon_{xx} - \varepsilon_{yy}$ of up to 4000 ppm in magnitude can be generated using a PMN-PT substrate with this composition and cut [20].

Micromagnetics simulations were run to validate the EA and HA locations of the 'peanut' shaped nanomagnet. This finite element based model uses the LLG equation with magnetoelastic coupling and shape demagnetization effects to simulate device behavior [36]. Ni properties used in simulation are $M_s = 4.8 \times 10^5 (\mathrm{A\,m^{-1}})$, $A_{\mathrm{ex}} = 1.05 \times 10^{-11} (\mathrm{J\,m^{-1}})$, $\alpha_{100} = -46 \times 10^{-6}$, $\alpha_{111} = -24 \times 10^{-6}$, $c_{11} = 2.5 \times 10^{11} (\mathrm{N\,m^{-2}})$, $c_{12} = 1.6 \times 10^{11} (\mathrm{N\,m^{-2}})$ and $c_{44} = 1.18 \times 10^{11} (\mathrm{N\,m^{-2}})$. The Gilbert damping constant was set as $\lambda = 0.5$ to improve model stability. During the design of the 'peanut' shape, five parameters were modified that to achieve the desired magnetic behavior: length of major axis L_{major}, length of minor axis L_{minor}, angle of major axis θ_{major}, angle of minor axis θ_{minor} and magnetic element thickness d. In the micromagnetics simulations presented, these parameters were set as $L_{\mathrm{major}} = 111$ nm, $L_{\mathrm{minor}} = 90$ nm, $\theta_{\mathrm{major}} = 60°$, $\theta_{\mathrm{minor}} = 45$ °and $d = 10$ nm. The energy profile of the 'peanut' shape is shown in Supplementary figure S1, with the EA along $\theta_{\mathrm{ea}} = 82.6°$ and HA along $\theta_{\mathrm{ha}} = 5.1°$. The EA and HA have been rotated CW and CCW respectively, compared to the energy profile of a standard ellipse shown in Supplementary figure S2 with $\theta_{\mathrm{ea}} = 90°$ and $\theta_{\mathrm{ha}} = 0°$. We note that for the 'peanut' shape θ_{ea} and θ_{ha} do not exactly align with θ_{major} and θ_{minor}. This can be better understood in terms of the energy profile of the device structure. The EA and HA of a system correspond to the magnetic energy minimum and maximum respectively. Further, the EA and HA are determined by the direction of the net magnetic moment and the energy associated with a magnetic structure that has a net magnetization slightly off the EA or HA will still have energy close to that of the extremum. So in reality the energy of a magnetic structure varies continuously and relatively smoothly as a 'function' of the angle of magnetization. In the

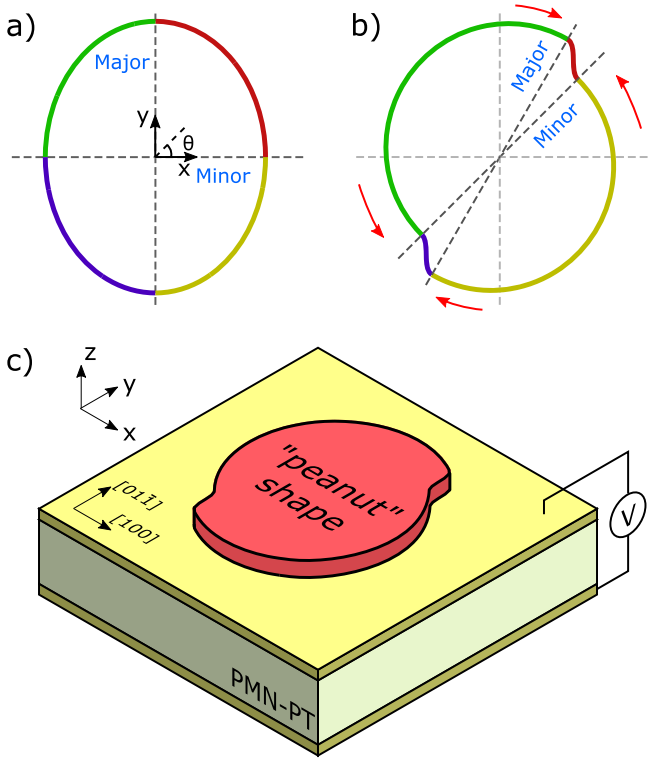

Figure 2. The design process of the 'peanut' shaped nanomagnet. (a) The shape of a standard ellipse, with EA and HA coincident with major axis along y-axis and minor axis along x-axis, respectively. (b) Moving the location of geometric major axis CW and minor axis CCW, aiming to rotate magnetic EA and HA accordingly and to produce non-perpendicular EA and HA. The shape in (b) is named 'peanut' shape due to geometric similarity. The four parts of the 'peanut' shape in (b) labeled in different color, are corresponding to the parts with same color in four quadrants in the ellipse in (a). (e) The isometric view of the strain-mediated ME device with the 'peanut' shaped nanomagnet on a PMN-PT substrate.

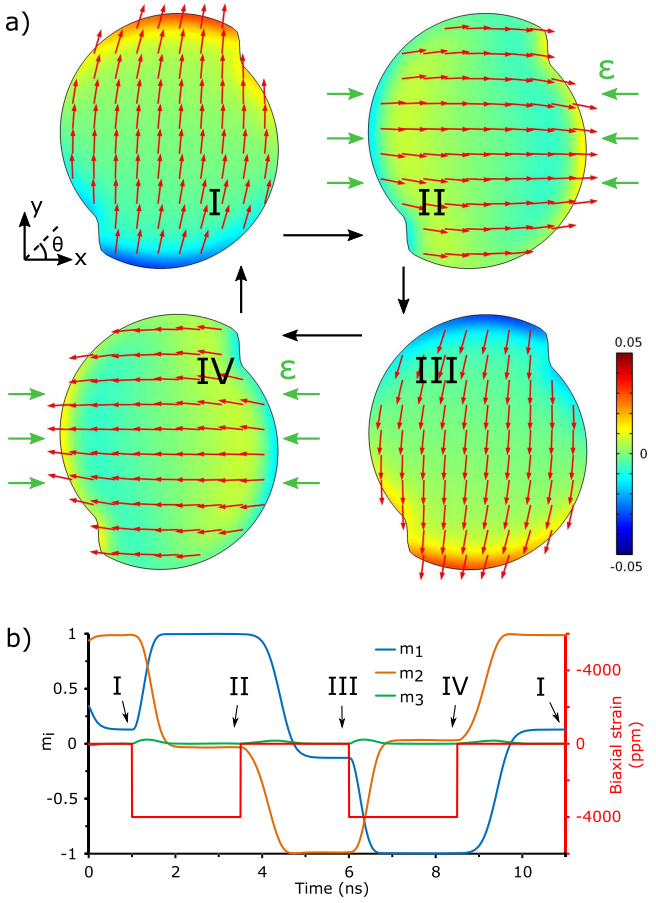

Figure 3. The micromagnetic simulation results of the 'peanut' shaped nanomagnet controlled by the electric-field-induced strain on the PMN-PT substrate. (a) Magnetization distribution in four states, I (before piezostrain was applied at $t = 1$ ns, and after piezostrain was applied twice at $t = 11$ ns), II (after piezostrain was applied at $t = 3.5$ ns), III (after piezostrain was released at $t = 6$ ns) and IV (after piezostrain was applied again at $t = 8.5$ ns). The red arrows represent the local in-plane magnetization direction. The rainbow background color indicates the out-of-plane component of local magnetization. Green arrows indicate the compressive strain direction of the applied piezoelectric biaxial strain. (b) The magnetization components change in response to the applied piezoelectric biaxial strain. m_1, m_2 and m_3 denote the averaged magnetization component along x, y and z axis, respectively. The solid red line indicates the applied biaxial strain loading as a function of time.

energy profile, valley floors and hill tops represent the EA and HA respectively. For this example the major axis and minor axis are 15° apart. This places a local minimum very close to a local maximum with the effect being that these two features distort each other, the net result being that the EA and HA determined by micromagnetics simulations are further apart than predicted from the geometry alone, i.e. at 82.6° and 5.1° respectively. The energy barrier between two stable magnetization states along EA is 263 k_bT, satisfying the suggested thermal stability requirement of non-volatile magnetic memory bit design (>40 k_bT) [40].

Figure 3(a) shows micromagnetics simulation results of the 'peanut' nanomagnet in response to the electric-field-induced strain on the piezoelectric substrate. The red arrows indicate the local in-plane magnetization direction. Background rainbow colors indicate the magnitude of out-of-plane magnetization. The magnetization of the 'peanut' nanomagnet was initialized along the θ_{major} direction at time $t = 0$. State I shows the magnetization distribution at time $t = 1$ ns when the magnetization stabilized and formed a single domain state aligned with the EA at $\theta_{\text{ea}} = 82.6°$. Piezoelectric biaxial strain of $\varepsilon_{xx} - \varepsilon_{yy} = -4000$ ppm was applied right after 1 ns at $1\text{ ns} < t \leqslant 3.5$ ns. State II shows the magnetization at $t = 3.5$ ns before piezostrain was released. The magnetization of the 'peanut' shape rotated CW towards the compressive strain direction (green arrows) and stabilized on average along $\theta = -1.9°$, indicating that this strain level is sufficient to eliminate the metastable state and induce magnetization rotation. The piezoelectric strain field was then released at $3.5\text{ ns} < t \leqslant 6$ ns. State III shows the magnetization at $t = 6$ ns. Relative to the state II with applied piezostrain, the magnetization rotated CW and stabilized on average in the direction of $\theta = -97.4°$ aligning with the EA. From state I to state III, the magnetization rotated CW 180° in total by applying and then releasing −4000 ppm piezoelectric biaxial strain. Similarly, the same strain field was again applied at $6\text{ ns} < t \leqslant 8.5$ ns and was released at $8.5\text{ ns} < t \leqslant 11$ ns. State IV demonstrated the magnetization distribution at

$t = 8.5$ ns. At $t = 11$ ns the magnetization distribution was the identical as the one in state I. This shows that the magnetization rotated back to the original state. The whole process of magnetization components m_1, m_2 and m_3 changing relative to time is illustrated in figure 3(b). During the 11 ns of the simulation, a 360° deterministic CW magnetization rotation (two sequential 180° rotations) was achieved by applying the same piezoelectric biaxial strain field twice. A movie of the magnetization response during $0\,\text{ns} \leqslant t \leqslant 11\,\text{ns}$ can be found at supplementary movie 1. The micromagnetics simulations demonstrate the function of the ME device with the engineered 'peanut' nanomagnet.

A parametric study of the 'peanut' shape magnetic element is shown in supplementary note 1. It is shown that changing either θ_{major} or θ_{minor} can move both θ_{ea} and θ_{ha}. The ratio of L_{minor} over L_{major}, and the thickness d determine the energy barrier between the EA and HA, and hence the magnitude of piezoelectric biaxial strain required to cross over that barrier to achieve 180° magnetization switching. The parameters can be further tuned to optimize the functionality of the device tailoring it to a particular application.

3. The 'cat-eye' shaped nanomagnet

The 'cat-eye' shaped nanomagnet was developed as an annular structure that can achieve deterministic strain-mediated electrically driven 180° magnetization reorientation on a piezoelectric substrate. For a typical symmetric ring nanomagnet, strain-mediated magnetization control is not deterministic and limited by 90° rotation. A narrow thin-film magnetic ring structure can form into an 'onion' domain state with two head-to-head domain walls [9, 20]. Due to its geometric center-symmetry composed of two concentric circles, a ring nanomagnet in the 'onion' state has no in-plane EA or HA, i.e., no preferred magnetization direction. Previous research has demonstrated that the magnetization of a ring structure can be rotated by 90° by electric-field-induced strain on a PMN-PT substrate, however the rotational direction is not deterministic [41]. Once applying the piezoelectric biaxial strain field to a ring nanomagnet with compressive strain direction orthogonal to the original magnetization direction, the magnetization has equal probability of rotating CW and CCW by 90°. When the piezostrain is released, the magnetization stays in this new orientation. A method for deterministic magnetization control in ring structures is required for device applications.

We start with introducing EA and HA into ring structures. A recent study by Richter *et al* experimentally demonstrated shape driven domain wall motion in an asymmetric permalloy ring structure (composed by two off-centered circles) from the geometric widest part to the narrowest part [42]. As a first step in taking advantage of this phenomenon, we performed micromagnetics simulations on a ring structure with the circular outer shape and elliptical inner shape shown in figures 4(a), (b). Note that in this geometry, there are two widest parts along the x-axis and two narrowest parts along the y-axis. Once the magnetization was initialized

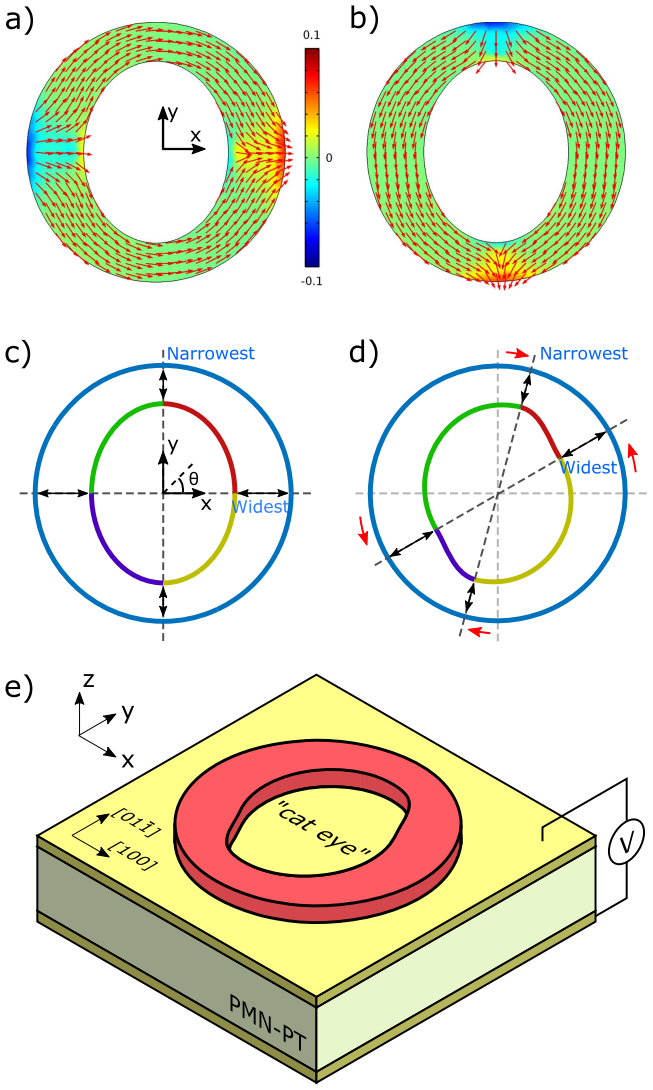

Figure 4. The design process of the 'cat-eye' shape magnetic element. (a) Micromagnetics simulation result of an asymmetric ring with circular outer shape (500 nm diameter) and elliptical inner shape (major axis 350 nm, minor axis 280 nm), initialized along x direction and formed 'onion' state. The red arrows represent local in-plane magnetization direction. The rainbow background color indicates the out-of-plane component of local magnetization. (b) Micromagnetics simulation result when magnetization fully relaxed and moved to lowest energy state. (c) The shape of an asymmetric ring with circular outer shape and elliptical inner shape. (d) Moving the location of two narrowest parts CW and two widest parts CCW in a ring structure, aiming to rotate magnetic EA and HA to produce non-perpendicular EA and HA. The four parts of the inner shape labeled in different color, are corresponding to the parts with same color in four quadrants in the inner ellipse in (c). (e) The isometric view of the strain-mediated ME device with the 'cat-eye' shaped nanomagnet on a PMN-PT substrate.

along the x-axis, the magnetization formed into the 'onion' state (see figure 4(a)) and automatically rotated to the two narrowest parts along the y-axis as shown in figure 4(b). The energy plot of this process (see supplementary figure S4) indicates that this results in minimization of the combined demagnetization energy and exchange energy. Since the magnetization direction tends towards the geometric

narrowest parts (y-axis) and away from the widest parts (x-axis), the x-axis can be considered a magnetic HA and the y-axis an EA for this outer-circular and inner-elliptical ring structure. Comparing with the symmetric ring structure composed of two concentric circles, we induced an EA and HA into the ring structure by modifying the inner shape from a circle to an ellipse. Note for this shape the EA and HA are perpendicular to each other.

We further modified the inner shape of the ring structure to achieve magnetic anisotropy with EA and HA non-perpendicular to each other (used also in 'peanut' shape design) to achieve the function of deterministic 180° magnetization rotation with a single piezostrain actuation. The mechanism bridging geometric shape and magnetic behavior is the shape driven domain wall motion away from geometric widest part (magnetic HA) and towards narrowest part (EA). Starting from the shape shown in figure 4(c), we moved the location of geometric widest parts CCW and narrowest parts CW, aiming to rotate the magnetic EA and HA. This produced a new shape as shown in figure 4(d). The four quadrants of the original inner elliptical shape correspond to the four parts with same color of the modified shape. This new shape is referred to as 'cat-eye' due to geometric similarity. Figure 4(e) shows the resultant design of the strain-mediated ME device on PMN-PT substrate. The PMN-PT substrate provides the required biaxial strain along its crystalline directions (compressive strain along [100] and tensile strain along $[01\bar{1}]$).

Micromagnetics simulations were performed to validate the 'cat-eye' shape design in response to the electric-field-induced strain on the PMN-PT substrate, shown in figure 5. There are six parameters that define the shape and affect the magnetic behavior of the 'cat-eye' shape element: length of outer shape diameter L_{outer}, width of the narrowest part of the ring $L_{\text{narrowest}}$, width of the widest part of the ring L_{widest}, angle of the narrowest part $\theta_{\text{narrowest}}$, angle of widest part θ_{widest} and magnetic structure thickness d. In this simulation, $L_{\text{outer}} = 500\,\text{nm}$, $L_{\text{narrowest}} = 75\,\text{nm}$, $L_{\text{widest}} = 120\,\text{nm}$, $\theta_{\text{narrowest}} = 75°$, $\theta_{\text{widest}} = 30°$ and $d = 15\,\text{nm}$. After magnetization is initialized along the $\theta_{\text{narrowest}}$ direction at $t = 0\,\text{ns}$, the magnetization formed into 'onion' state and stabilized at $t = 0.5\,\text{ns}$. Two head-to-head domain walls formed at $\theta = 75°$ and $-105°$ position respectively, see state I in figure 5(a). A piezoelectric biaxial strain of $\varepsilon_{xx} - \varepsilon_{yy} = -4000\,\text{ppm}$ was applied at $0.5\,\text{ns} < t \leqslant 23\,\text{ns}$. State II shows the magnetization distribution at $t = 23\,\text{ns}$. After application of piezostrain, it can be seen that the domain walls align with the compressive strain (green arrows) direction at $\theta = 0°$. From $23\,\text{ns} < t \leqslant 50\,\text{ns}$, the piezostrain was released and state III shows the resultant magnetization distribution at $t = 50\,\text{ns}$. It is shown that the magnetization continued to rotate CW until stopping at the position 180° from the initial condition in state I. This is due to an energy minimization process involving demagnetization energy and exchange energy. An energy plot for this process is shown in Supplementary figure S6. From time $t = 0$ to $t = 50\,\text{ns}$, the magnetization of the 'cat-eye' shape rotated CW by 180° with a single application of piezostrain. The same biaxial strain

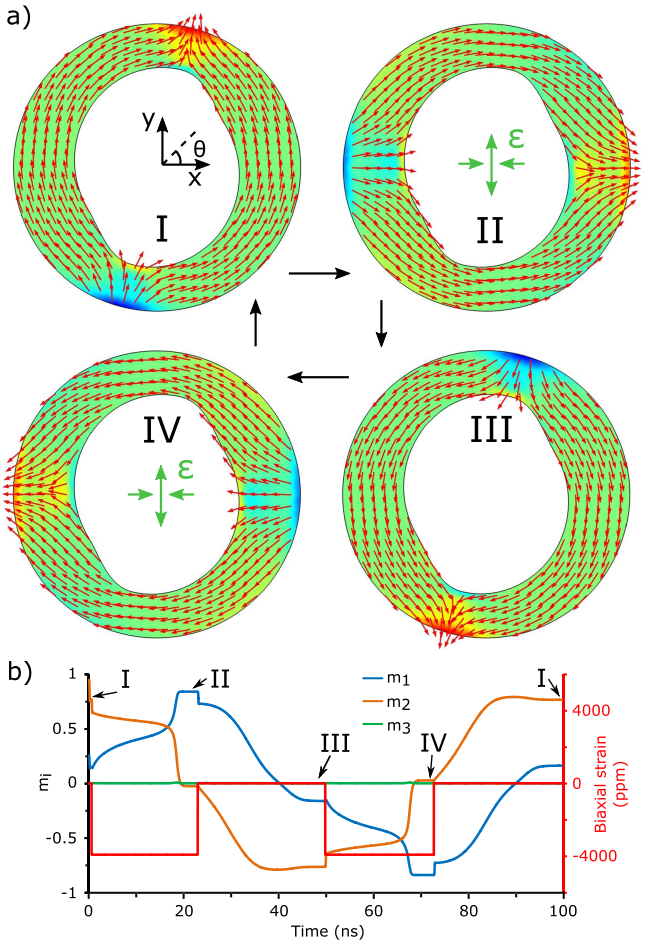

Figure 5. The micromagnetics simulation results of the 'cat-eye' shaped nanomagnet controlled by electric-field-induced strain on the PMN-PT substrate. (a) Magnetization distribution in four states, I (before piezostrain was applied at $t = 0.5\,\text{ns}$, and after piezostrain was applied twice at $t = 100\,\text{ns}$), II (after piezostrain was applied at $t = 23\,\text{ns}$), III (after piezostrain was released at $t = 50\,\text{ns}$) and IV (after piezostrain was applied again at $t = 73\,\text{ns}$). The red arrows represent the local in-plane magnetization direction. The rainbow background color indicates the out-of-plane component of local magnetization. Green arrows indicate the direction of the applied piezoelectric biaxial strain. (e) The magnetization components change in response to the applied piezoelectric biaxial strain. m_1, m_2 and m_3 denote the averaged magnetization component along x, y and z-axis, respectively. The solid red line indicates the applied biaxial strain loading as a function of time.

was applied at $50\,\text{ns} < t \leqslant 73\,\text{ns}$ and released at $73\,\text{ns} < t \leqslant 100\,\text{ns}$. State IV shows the magnetization distribution at $t = 73\,\text{ns}$. At $t = 100\,\text{ns}$ the magnetization went back to its original state I before any strain was applied. This confirms that the second application of piezostrain deterministically drove the magnetization through a second 180° CW rotation. Overall, a 360° magnetization rotation was achieved from $t = 0\,\text{ns}$ to $100\,\text{ns}$ during which the piezostrain was applied twice. The magnetization components m_1, m_2 and m_3 in response to piezoelectric biaxial strain are plotted in figure 5(b). During the 100 ns of simulation, a 360° deterministic CW magnetization rotation was achieved from two subsequent 180° rotations, each induced by application of the same piezoelectric strain field. A movie of the magnetization

response during 0 ns $\leqslant t \leqslant$ 100 ns can be found at supplementary movie 2. The micromagnetics simulations demonstrate the function of the ME device with the engineered 'cat-eye' nanomagnet.

The design parameters L_{outer}, $L_{narrowest}$, L_{widest}, $\theta_{narrowest}$, θ_{widest} and d can be changed and optimized according to target device function. The 'cat-eye' shape has a wide range of scalability, since the 'onion' state exists among magnetic rings with outer diameter from a few hundred nanometers up to a few microns. By changing the strain rate of the applied load, the speed of domain wall motion can be controlled. The relative positions of the two widest/narrowest ring sections do not have to be center-symmetric for a functioning device. The wide availability of the design parameters increases the applicability of the 'cat-eye' shape nanomagnets for various spintronic devices.

4. Engineering principles

The engineering principles we followed in designing the 'peanut' and 'cat-eye' shapes are summarized. The conventional approach for nanomagnetic device research is: (1) bring up a nanomagnet in a certain shape; (2) investigate its magnetic anisotropy; and (3) design a device with this nanomagnet for a certain function. In this article, we adopted a reversed approach: (1) design a nanomagnetic device with a certain function (180° magnetization switching in response to a single piezostrain pulse); (2) determine the desired magnetic anisotropy (EA and HA not perpendicular to each other) that leads to this type of functionality; and (3) architect the shape of the nanomagnet to obtain this magnetic anisotropy (through the mechanism bridging geometric shape and magnetic behavior). Since the new approach provides a guideline for engineering novel shapes for a targeted device function, only a few micromagnetics simulations are needed to fine tune the design and produce a shape with the desired functionality.

This idea of engineering nanomagnets in novel shapes could be implemented with computer-assisted topological optimization techniques. The 'peanut' shape parametric study (see supplementary note 1) has demonstrated that varying the geometric shape parameters (L_{major}, L_{minor}, θ_{major}, θ_{minor} and d) can affect the function of the device. These shape parameters can be optimized. The optimization rules can be set as tailored magnetic anisotropy, thermal stability requirement ($>40\,k_bT$), certain amount of applied magnetic field/piezostrain/spin-polarized current and magnetization switching time, etc. After the topological optimization process, engineers can find improved nanomagnet designs with optimized device performance.

5. Discussion

In this article, we architected the shape of nanomagnets with tailored magnetization behavior. We presented novel 'peanut' and 'cat-eye' shaped nanomagnets, both demonstrating the ability to accomplish strain-mediated CW 180° magnetization rotation like magnetic ratchets. Magnetic anisotropy with non-perpendicular EA and HA can achieve deterministic 180° magnetization switching in response to piezoelectric biaxial strain. In order to incorporate this type of magnetic anisotropy in nanomagnets, we modified the geometric shape based on the mechanism bridging geometry and magnetic behavior. The 'peanut' and 'cat-eye' shapes were then produced. A strain-mediated ME device was designed with the 'peanut' and 'cat-eye' shaped nanomagnets and a PMN-PT piezoelectric substrate. Micromagnetics simulations were employed and the results demonstrated the performance of the device, achieving deterministic CW 180° magnetization rotation upon a single piezostrain pulse, and a total of 360° magnetization rotation by applying the same strain field twice.

A number of challenges have been encountered by the authors in the development of similar sized ring structures. High resolution electron beam (e-beam) lithography is required to precisely define the shape of the nanomagnets. PMN-PT tends to accumulate charges during lithography due to its dielectric properties. These charges were found to deflect the e-beam, inducing an ill-defined structure with notches as magnetic pinning sites. To dissipate the charges, a conductive layer (e.g., 5 nm of Au) sputtered above the e-beam resist is suggested. Besides, orientation of the nanomagnets needs to be accurately aligned with the PMN-PT substrate, with EA and HA in between the compressive and tensile strain directions. However, the alignment may fail due to the piezoelectric domains (about 1 μm in size) on piezoelectric substrate, providing uncertain strain magnitude and direction for nanomagnets deposited on these domains [14]. A thick (several microns) and relatively soft strain-mitigation layer deposited above the PMN-PT and electrodes may average the various strain fields from piezoelectric domains. Nanomagnets could be fabricated on top of this layer. These development efforts are ongoing.

The 'peanut' and 'cat-eye' shaped nanomagnets provide a simple and effective design for developing future spintronic devices, e.g. non-volatile memory bits. The engineering principle implemented in this article starts from a target device function down to nanomagnets in novel shapes. This method may be coupled with topology optimization techniques to achieve optimized nanomagnet shapes. This approach opens a broad design space for next generation spintronic devices with nanomagnets in novel shapes taking advantage of magnetic shape anisotropy.

Acknowledgements

This work was supported by NSF Nanosystems Engineering Research Center for Translational Applications of Nanoscale Multiferroic Systems (TANMS) Cooperative Agreement Award (No. EEC-1160504).

References

[1] Nan C W, Bichurin M I, Dong S, Viehland D and Srinivasan G 2008 Multiferroic magnetoelectric composites: historical perspective, status, and future directions *J. Appl. Phys.* **103** 031101

[2] Hu J-M, Li Z, Chen L-Q and Nan C-W 2011 High-density magnetoresistive random access memory operating at ultralow voltage at room temperature *Nat. Commun.* **2** 553

[3] Wolf S A, Awschalom D D, Buhrman R A, Daughton J M, von Molnár S, Roukes M L, Chtchelkanova A Y and Treger D M 2001 Spintronics: a spin-based electronics vision for the future *Science* **294** 1488–95

[4] Atulasimha J and Bandyopadhyay S 2016 Introduction to spintronic and nanomagnetic computing devices *Nanomagnetic and Spintronic Devices for Energy-Efficient Memory and Computing* (New York: Wiley) pp 1–8

[5] O'handley R C 2000 *Modern Magnetic Materials: Principles and Applications* (New York: Wiley)

[6] Hehn M, Ounadjela K, Bucher J, Rousseaux F, Decanini D, Bartenlian B and Chappert C 1996 Nanoscale magnetic domains in mesoscopic magnets *Science* **272** 1782–5

[7] Cowburn R P 1999 Property variation with shape in magnetic nanoelements *J. Phys. D: Appl. Phys.* **33** R1–16

[8] Rothman J, Kläui M, Lopez-Diaz L, Vaz C A F, Bleloch A, Bland J A C, Cui Z and Speaks R 2001 Observation of a bi-domain state and nucleation free switching in mesoscopic ring magnets *Phys. Rev. Lett.* **86** 1098–101

[9] Kläui M, Vaz C A F, Lopez-Diaz L and Bland J A C 2003 Vortex formation in narrow ferromagnetic rings *J. Phys.: Condens. Matter* **15** R985

[10] Gopman D B, Kabanov Y P, Cui J, Lynch C S and Shull R D 2016 Influence of internal geometry on magnetization reversal in asymmetric permalloy rings *Appl. Phys. Lett.* **109** 082407

[11] Muñoz-Sandoval E, Torres-Heredia J J and López-Urías F 2005 Micromagnetic simulations of hysteresis loops in ferromagnetic Reuleaux's triangles *J. Appl. Phys.* **97** 80–3

[12] Imre A, Csaba G, Ji L, Orlov A, Bernstein G H and Porod W 2006 Majority logic gate for magnetic quantum-dot cellular automata *Science* **311** 205–8

[13] Lambson B, Carlton D and Bokor J 2011 Exploring the thermodynamic limits of computation in integrated systems: magnetic memory, nanomagnetic logic, and the landauer limit *Phys. Rev. Lett.* **107** 010604

[14] Buzzi M, Chopdekar R V, Hockel J L, Bur A, Wu T, Pilet N, Warnicke P, Carman G P, Heyderman L J and Nolting F 2013 Single domain spin manipulation by electric fields in strain coupled artificial multiferroic nanostructures *Phys. Rev. Lett.* **111** 027204

[15] Carlton D B, Emley N C, Tuchfeld E and Bokor J 2008 Simulation studies of nanomagnet-based logic architecture *Nano Lett.* **8** 4173–8

[16] Kläui M, Vaz C A F, Bland J A C, Wernsdorfer W, Faini G and Cambril E 2003 Domain wall pinning and controlled magnetic switching in narrow ferromagnetic ring structures with notches (invited) *J. Appl. Phys.* **93** 7885–90

[17] Bisig A *et al* 2013 Correlation between spin structure oscillations and domain wall velocities *Nat. Commun.* **4** 2328

[18] Zhu J-G, Zheng Y and Prinz G A 2000 Ultrahigh density vertical magnetoresistive random access memory (invited) *J. Appl. Phys.* **87** 6668

[19] Rapoport E and Beach G S D 2012 Dynamics of superparamagnetic microbead transport along magnetic nanotracks by magnetic domain walls *Appl. Phys. Lett.* **100** 082401

[20] Sohn H *et al* 2015 Wall rotation in multiferroic heterostructures to manipulate suspended on-chip magnetic particles *ACS Nano* **9** 4814–26

[21] Hu J M and Nan C W 2009 Electric-field-induced magnetic easy-axis reorientation in ferromagnetic/ferroelectric layered heterostructures *Phys. Rev.* B **80** 224416

[22] Wang J J, Hu J M, Ma J, Zhang J X, Chen L Q and Nan C W 2014 Full 180° magnetization reversal with electric fields *Sci. Rep.* **4** 7507

[23] Iwasaki Y 2002 Stress-driven magnetization reversal in magnetostrictive films with in-plane magnetocrystalline anisotropy *J. Magn. Magn. Mater.* **240** 395–7

[24] Roy K, Bandyopadhyay S and Atulasimha J 2013 Binary switching in a 'symmetric' potential landscape *Sci. Rep* **3** 3038

[25] Hu J, Yang T, Wang J, Huang H, Zhang J, Chen L and Nan C 2015 Purely electric-field-driven perpendicular magnetization reversal *Nano Lett.* **15** 616–22

[26] Li X, Carka D, Liang C, Sepulveda A E, Keller S M, Amiri P K, Carman G P and Lynch C S 2015 Strain-mediated 180° perpendicular magnetization switching of a single domain multiferroic structure *J. Appl. Phys.* **118** 014101

[27] Cui J, Hockel J L, Nordeen P K, Pisani D M, Liang C, Carman G P and Lynch C S 2013 A method to control magnetism in individual strain-mediated magnetoelectric islands *Appl. Phys. Lett.* **103** 232905

[28] Liang C-Y, Keller S M, Sepulveda A E, Sun W-Y, Cui J, Lynch C S and Carman G P 2014 Electrical control of a single magnetoelastic domain structure on a clamped piezoelectric thin film—analysis *J. Appl. Phys.* **116** 123909

[29] Peng R-C, Wang J J, Hu J-M, Chen L-Q and Nan C-W 2015 Electric-field-driven magnetization reversal in square-shaped nanomagnet-based multiferroic heterostructure *Appl. Phys. Lett.* **106** 142901

[30] Cui J, Liang C-Y, Paisley E A, Sepulveda A, Ihlefeld J F, Carman G P and Lynch C S 2015 Generation of localized strain in a thin film piezoelectric to control individual magnetoelectric heterostructures *Appl. Phys. Lett.* **107** 092903

[31] Liang C-Y, Sepulveda A E, Hoff D, Keller S M and Carman G P 2015 Strain-mediated deterministic control of 360° domain wall motion in magnetoelastic nanorings *J. Appl. Phys.* **118** 174101

[32] Hu J-M *et al* 2016 Fast magnetic domain-wall motion in a ring-shaped nanowire driven by a voltage *Nano Lett.* **16** 2341–8

[33] Banas L 2005 Numerical methods for the Landau–Lifshitz–Gilbert equation *Numerical Analysis and Its Applications: 3rd Int. Conf., NAA 2004 (Rousse, Bulgaria, 29 June–3, July 2004)* ed Z Li (Berlin: Springer) pp 158–65 revised selected papers

[34] Shu Y C, Lin M P and Wu K C 2004 Micromagnetic modeling of magnetostrictive materials under intrinsic stress *Mech. Mater.* **36** 975–97

[35] Zhang J X and Chen L Q 2005 Phase-field microelasticity theory and micromagnetic simulations of domain structures in giant magnetostrictive materials *Acta Mater.* **53** 2845–55

[36] Liang C-Y, Keller S M, Sepulveda A E, Bur A, Sun W-Y, Wetzlar K and Carman G P 2014 Modeling of magnetoelastic nanostructures with a fully coupled mechanical-micromagnetic model *Nanotechnology* **25** 435701

[37] Ross C A *et al* 2002 Magnetic behavior of lithographically patterned particle arrays (invited) *J. Appl. Phys.* **91** 6848

[38] Cowburn R P, Koltsov D K, Adeyeye A O and Welland M E 1999 Single-domain circular nanomagnets *Phys. Rev. Lett.* **83** 1042–5

[39] Wu T, Bur A, Zhao P, Mohanchandra K P, Wong K, Wang K L, Lynch C S and Carman G P 2011 Giant electric-field-induced reversible and permanent magnetization reorientation on magnetoelectric Ni/(011) [Pb (Mg1/3 Nb 2/3) O3](1-*x*)-[PbTiO3] *x* heterostructure *Appl. Phys. Lett.* **98** 012504

[40] Zhu J-G 2008 Magnetoresistive random access memory: the path to competitiveness and scalability *Proc. IEEE* **96** 1786–98

[41] Hockel J L, Bur A, Wu T, Wetzlar K P and Carman G P 2012 Electric field induced magnetization rotation in patterned Ni ring/Pb(Mg1/3Nb2/3)O3](1−0.32)-[PbTiO3]0.32 heterostructures *Appl. Phys. Lett.* **100** 022401

[42] Richter K, Mawass M, Krone A, Kruger B, Weigand M, Schutz G, Stoll H and Klaeui M 2015 Automotive domain wall propagation in ferromagnetic rings *2015 IEEE Magn. Conf. (INTERMAG)* p 1